Molecular Crystals and Liquid Crystals

ISSN: (Print) (Online) Journal homepage: https://www.tandfonline.com/loi/gmcl20

Liquid crystalline behaviors of three series of hockey stick-like compounds

Gege Jin, Yongmin Guo, Limin Wu, Yi Li, Baozong Li & Yonggang Yang

To cite this article: Gege Jin, Yongmin Guo, Limin Wu, Yi Li, Baozong Li & Yonggang Yang (2020) Liquid crystalline behaviors of three series of hockey stick-like compounds, Molecular Crystals and Liquid Crystals, 709:1, 1-13, DOI: 10.1080/15421406.2020.1811015

To link to this article: https://doi.org/10.1080/15421406.2020.1811015

MOLECULAR CRYSTALS AND LIQUID CRYSTALS
2020, VOL. 709, NO. 1, 1–13
https://doi.org/10.1080/15421406.2020.1811015

Liquid crystalline behaviors of three series of hockey stick-like compounds

Gege Jin[a], Yongmin Guo[a], Limin Wu[b], Yi Li[a], Baozong Li[a], and Yonggang Yang[a]

[a]Jiangsu Key Laboratory of Advanced Functional Polymer Design and Application, Department of Polymer Science and Engineering, State and Local Joint Engineering Laboratory for Novel Functional Polymeric Materials, College of Chemistry, Chemical Engineering and Materials Science, Soochow University, Suzhou, P. R. China; [b]School of Environmental Science and Engineering, Yancheng Institute of Technology, Yancheng, Jiangsu Province, P. R. China

ABSTRACT
Three series of *meta*-perfluoroalkylphenol esters are synthesized. Both SmA and SmC phases are identified. Their clearing points increase with increasing the perfluorocarbon chain length, while decrease with increasing the alkoxy chain length. Comparison of the 3-tridecafluorohexylbenzoates and 3-tridecafluorohexylphenol esters, the 3-tridecafluorohexylbenzoates show higher clearing points, indicating that the direction of the ester bond plays an important role in the thermostability of the liquid crystalline phases. Moreover, it was proposed that the compounds with short and long alkoxy chains packed into different structures.

KEYWORDS
Ester; lateral substitution; liquid crystal; perfluoroalkyl

Introduction

Liquid crystals with varieties of geometric structures, such as rod-like, bowl-shaped, banana-shaped, T-shaped have been developed. Among these structures, rod-like liquid crystals have been well-studied. For the liquid crystals with perfluoroalkyl and semi-perfluoroalkyl chains, most of them are rod-like molecules with fluorocarbon chains at the terminals [1–14]. Due to the fluorophilic association of the fluoroalkyl chains, smectic phases are feasible to be formed. With the introduction of chiral center, liquid crystals with wide temperature range of the SmC* phase can be obtained. Up to now, the reports on liquid crystals with lateral fluorocarbon chains are few [15–19]. T-shaped molecules with lateral fluorocarbon chains can organize into varieties of liquid crystalline phase [15–18]. *Meta*-perfluoroalkyl benzoates exhibit SmA, SmC, and SmB phases [19]. Herein, three series of hockey stick-like *meta*-perfluoroalkyl phenol esters were synthesized. Enantiotropic SmC phase preferred to be formed.

Results and discussion

The compounds, **F6OBP***n*, **F8OBP***n*, and **F10OBP***n*, were synthesized according to the route depicted in Scheme 1. The phase transition behavior of the final compounds is

CONTACT Y. Yang ygyang@suda.edu.cn; B. Li libaozong@suda.edu.cn Jiangsu Key Laboratory of Advanced Functional Polymer Design and Application, Department of Polymer Science and Engineering, State and Local Joint Engineering Laboratory for Novel Functional Polymeric Materials, College of Chemistry, Chemical Engineering and Materials Science, Soochow University, Suzhou 215123, P. R. China.

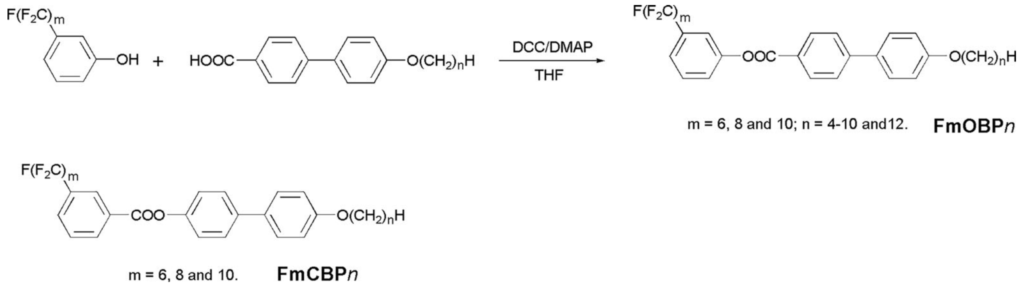

Scheme 1. Synthetic route of the compounds **FmOBP*n*** and molecular structures of **FmCBP*n***.

summarized in Table 1, which is mainly determined with differential scanning calorimetry (DSC). Since the enthalpies of the SmA-SmC and SmC-SmA transitions are low, the transition temperatures of them are failed to be obtained using DSC. Therefore, few data are obtained from polarizing optical microscopy (POM) characterization. Moreover, since the temperature ranges of the SmA phases of **F6OBP*4*** and **F8OBP*4*** are narrow, few date are also obtained from POM characterization. Figure 1 plots the transition temperatures of the compounds, **F6OBP*n***, **F8OBP*n***, and **F10OBP*n***, as a function of the number of methylene units (*n*) in the alkoxy chain. Only smectic phases were identified. For compounds **F6OBP*n***, enantiotropic SmC phase prefers to be formed (Fig. 1a). **F6OBP*4*** shows enantiotropic SmA and SmC phases and a monotropic CrE phase. The fan-shaped texture, broken fan-shaped one and fan-shaped one with arcs were identified in the POM images (Fig. 2). The others show only an enantiotropic SmC phase. The clearing points of this series show somewhat odd–even effect. Comparison of compounds **F6OBP*n*** and **F6CBP*n***, when the carbon number is same, the clearing point of **F6CBP*n*** is about 30K higher than that of **F6OBP*n*** (Scheme 1 and Fig. 1d). This phenomenon is proposed to be driven by the molecular polarity.

For compounds **F8OBP*n***, **F8OBP*4*** shows both enantiotropic SmA and SmC phases, and **F8OBP*10*** and **F8OBP*12*** show only a monotropic SmC phase (Fig. 1b). The others show only an enantiotropic SmC phase. The clearing points also show somewhat odd–even effect. For compounds **F10OBP*n***, **F10OBP*7*** shows a monotropic SmC phase, and the liquid crystalline behavior of **F10OBP*12*** could not be found due to recrystallization (Fig. 1c). The others are liquid crystals with an enantiotropic SmC phase. Comparison of these three series, with increasing the fluorocarbon chain length, both the melting point and clearing point are increased. However, the temperature range of the SmC phase becomes narrower. With increasing the length of the alkoxy chain, the clearing points decrease gradually, SmA phase is suppressed and SmC phase tends to be formed.

The phase transition behavior of compounds **F6CBP*8***, **F8CBP*8***, and **F10CBP*8*** has been reported previously [19]. With increasing the fluorocarbon chain length, the clearing points increase gradually, and SmC phase is suppressed (Fig. 3). Comparison of the compounds shown in Fig. 3, the 3-perfluoroalkylbenzoates show higher melting points and clearing points. The direction of the ester bond plays an important role in the mesophase structure, melting point and clearing point. A similar phenomenon has been reported previously [20].

The mesophases of the liquid crystals were further confirmed by characterizing using small angle X-ray scattering (SAXS) (Fig. 4). For **F6OBP*4***, the layer thicknesses are

Table 1. Transition temperatures of the compounds.

Compound	*n*	Transition temperature (°C)/ [Δ*H*] (kJ mol^{-1})
F6OBP_4_	_4_	Cr 105.4 [−16.49] SmC 142.9[a] SmA 148.5[a] I 148.3[a] SmA 142.7[a] SmC 98.9[a] CrE 82.9 [13.04] Cr
F6OBP_5_	_5_	Cr 97.0 [−15.58] SmC 134.1 [−11.05] I 129.9 [10.81] SmC 78.3 [14.17] Recr
F6OBP_6_	_6_	Cr 84.5 [−14.09] SmC 127.7 [−10.70] I 123.1 [11.13] SmC 60.7 [17.79] Recr
F6OBP_7_	_7_	Cr 94.6 [−24.94] SmC 115.3 [−9.27] I 111.5 [10.68] SmC 48.0 [16.03] Recr
F6OBP_8_	_8_	Cr 78.7 [−21.65] SmC 108.8 [−9.04] I 103.3 [10.27] SmC 42.7 [17.67] Recr
F6OBP_9_	_9_	Cr 93.0 [−20.23] SmC 101.7 [−5.11] I 97.6 [11.07] SmC 66.9 [25.41] Recr
F6OBP_10_	_10_	Cr 94.7 [−40.46] SmC 96.8 [−1.95] I 93.0 [10.00] SmC 76.5 [30.13] Recr
F6OBP_12_	_12_	Cr 88.8 [−0.65] SmC 91.3 [−38.97] I 84.1 [8.64] SmC 76.6 [25.69] Recr
F8OBP_4_	_4_	Cr 128.5 [−19.73] SmC 157.7[a] SmA 159.8[a] I 159.6[a] SmA 157.5[a] SmC 98.1 [17.41] Recr
F8OBP_5_	_5_	Cr 100.1 [−16.26] SmC 146.2 [−11.87] I 142.4 [16.78] SmC 66.8 [12.40] Recr
F8OBP_6_	_6_	Cr 117.2 [−28.16] SmC 137.8 [−10.03] I 133.8 [15.19] SmC 74.0 [13.89] Recr
F8OBP_7_	_7_	Cr 120.9 [−37.73] SmC 128.4 [−10.38] I 124.5 [14.85] SmC 71.7 [32.99] Recr
F8OBP_8_	_8_	Cr 102.2 [−32.46] SmC 121.8 [−10.83] I 118.1 [12.07] SmC 77.2 [18.48] Recr
F8OBP_9_	_9_	Cr 103.7 [−31.07] SmC 115.2 [−9.83] I 111.2 [13.29] SmC 81.2 [26.78] Recr
F8OBP_10_	_10_	Cr 109.4 [−46.24] I 106.0 [10.84] SmC 88.1 [32.10] Recr
F8OBP_12_	_12_	Cr 103.2 [−36.53] I 98.2 [10.33] SmC 88.5 [25.21] Recr
F10OBP_4_	_4_	Cr 152.5 [−28.37] SmC 161.7 [−9.06] I 158.3 [13.79] SmC 127.0 [25.21] Recr
F10OBP_5_	_5_	Cr 140.0 [−47.38] SmC 152.6 [−9.46] I 148.8 [11.49] SmC 107.3 [21.43] Recr
F10OBP_6_	_6_	Cr 141.0 [−22.02] SmC 145.9 [−2.68] I 141.7 [14.59] SmC 106.8 [34.38] Recr
F10OBP_7_	_7_	Cr 141.6 [−56.46] I 134.4 [12.51] SmC 106.7 [36.26] Recr
F10OBP_8_	_8_	Cr 117.5 [−27.08] SmC 132.4 [−11.20] I 128.9 [11.35] SmC 109.3 [26.11] Recr
F10OBP_9_	_9_	Cr 115.4 [−22.87] SmC 127.4 [−10.12] I 122.7 [12.58] SmC 107.0 [24.47] Recr
F10OBP_10_	_10_	Cr 121.0 [−2.33] SmC 122.4 [−39.09] I 117.7 [8.35] SmC 112.7 [25.04] Recr
F10OBP_12_	_12_	Cr 120.8 [−46.75] I 113.8 [48.21] Recr

Cr = crystal; SmC = smectic C; SmA = smectic A; I = isotropic liquid; CrE = crystal E; Recr = Recrystal.

[a] The data are obtained from POM characterization, and corresponding enthalpies, Δ*H* in kJ mol^{-1} detected on the second temperature run at a rate of 10 °C min^{-1}.

2.96, 2.94, and 3.11 nm at the SmA, SmC, and CrE mesophases, respectively. For the CrE mesophase, three peaks were identified at 3.11, 2.20, and 1.56 nm with a 1/*d* ratio of 1:$\sqrt{}^{\backslash\mathrm{bar}}$2:2. For the SAXS pattern of **F6OBP**_6_ taken at 110 °C, two peaks were identified at 2.91 and 1.46 nm, indicating a SmC mesophase. The layer thicknesses of the SmC mesophases of **F6OBP**_4_ and **F6OBP**_6_ were similar. However, for the SAXS pattern of **F6OBP**_9_ taken at 95 °C, one peak was identified at 3.16 nm. Similar phenomenon was also identified in the series of **F8OBP**_n_. The layer thicknesses of the SmC mesophases of **F8OBP**_4_ and **F8OBP**_6_ were 3.22 and 3.21 nm, respectively. However, layer thickness of the SmC mesophases of **F8OBP**_9_ was 3.32 nm. Moreover, for the SAXS pattern of **F10OBP**_4_ taken at 155 °C, one peak was identified at 3.65 nm, indicating a SmC mesophase with a layer thickness of 3.65 nm.

For the compounds **F6OBP**_7_, **F8OBP**_7_, and **F10OBP**_7_, comparison with their neighbors, the temperature ranges of their liquid crystalline phases are the narrowest. The molecular packing structures of the compounds shown in Table 1 seem to be different with increasing the alkoxy chain length. SAXS patterns of the compounds **F10OBP**_6_ and **F10OBP**_9_ were taken after being cooling down to 140 and 120 °C, respectively (Fig. 3). SmC phases were formed at these temperatures. Although the alkoxy chain lengths of the compounds **F10OBP**_6_ and **F10OBP**_9_ are different, the first scattering peaks of them are almost identical. Therefore, the molecular packing structures of them are proposed to be different [2,21,22]. The calculated molecular lengths of the compounds **F10OBP**_6_ and **F10OBP**_9_ are 3.68 and 4.01 nm, respectively. Since they are longer than the layer thickness, the molecules should show bent conformations and tilt within the layers. For the compound **F10OBP**_6_, neighboring molecules are proposed to organize

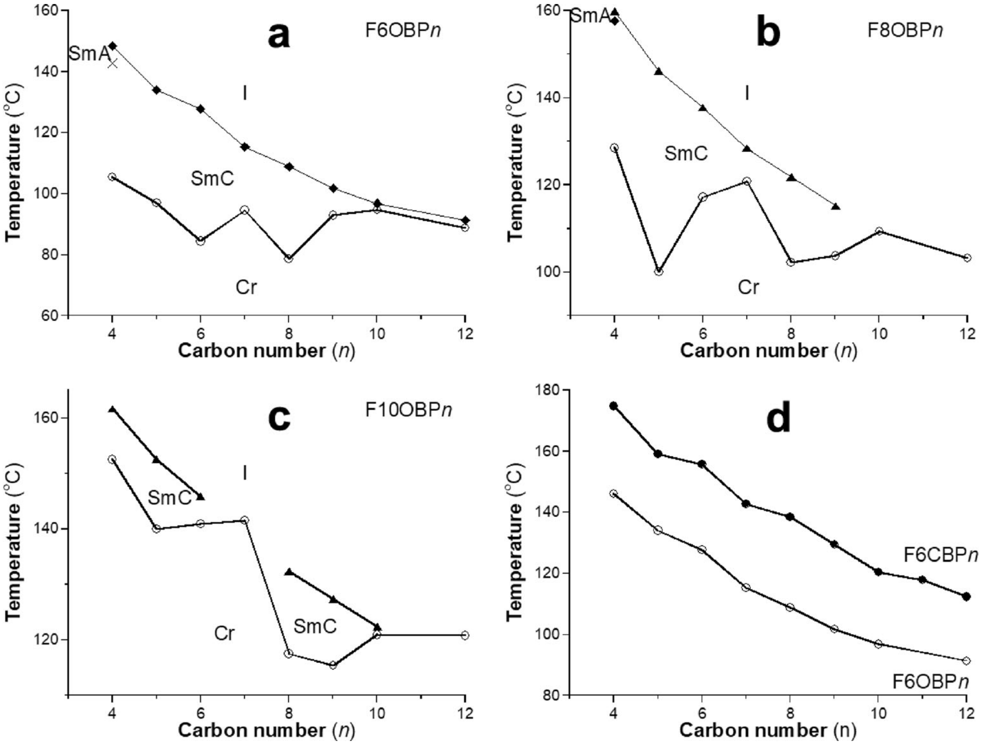

Figure 1. Transition behavior of the compounds (a) **F6OBP***n*, (b) **F8OBP***n* and (c) **F10OBP***n* in the heating process: dependence of the transition temperatures on the number (*n*) of methylene units of the non-fluorinated chain; (d) the clearing points of **F6OBP***n* and **F6CBP***n*.

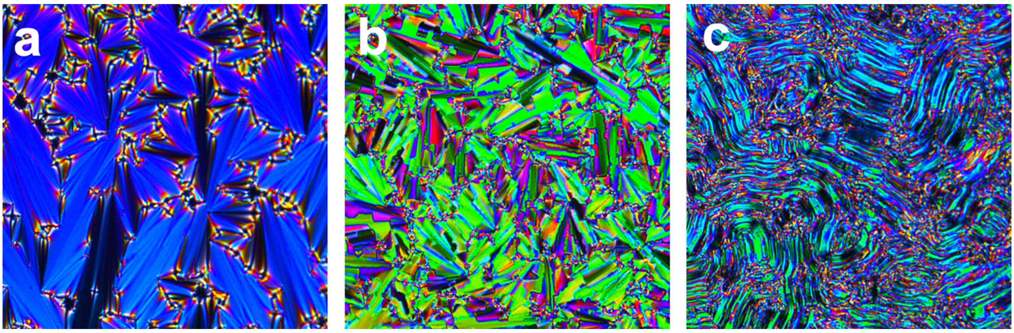

Figure 2. POM images of **F6OBP***4* taken during the cooling process. (a) The fan-shaped SmA texture taken at 148.0 °C; (b) broken fan-shaped SmC texture taken at 130.0 °C; (c) fan-shaped CrE texture with arcs taken at 85.0 °C.

antiparallel (Fig. 5a). The mainly driven forces should be the dipolar interactions between the antiparallel carbonyl groups. For the compound **F10OBP***9*, the molecules are proposed to organize in quasi-parallel (Fig. 5b) [21]. The hydrophobic association of hydrocarbon chains, the fluorophilic association of the fluorocarbon chains and the π-π/C–H … π interactions between neighboring aromatic rings should be the driven forces for the formation of this structure.

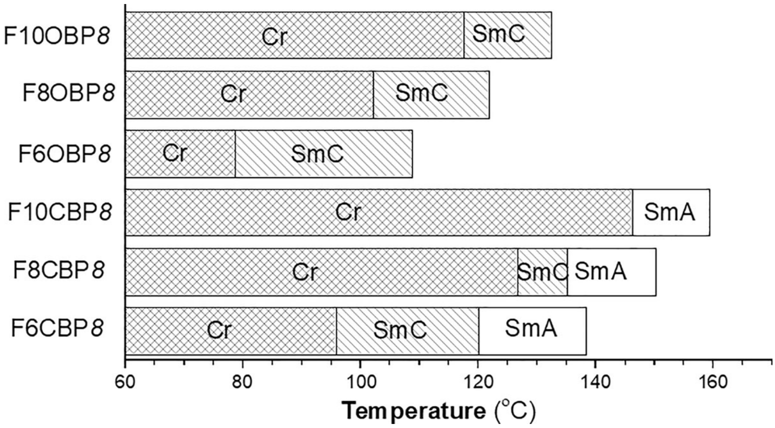

Figure 3. Transition behavior of the compounds **F6OBP***8*, **F8OBP***8*, **F10OBP***8*, **F6CBP***8*, **F8CBP***8*, and **F10CBP***8* in the heating process.

Conclusion

Three series of hockey stick-like compounds with perfluoroalkyl chains were synthesized. Most of them show an enantiotropic SmC phase. The clearing points decrease with increasing the alkoxy chain length and increase with increasing the perfluoroalkyl chain length. Both the liquid crystalline behavior and SAXS characterization suggested that the alkoxy chain length played an important role in the molecular packing structure at the SmC phase.

Experimental

Characterization

FT-IR spectra were performed on a VERTEX 70 spectrometer at 4 cm^{-1} resolution by averaging over 16 scans. The ^{1}H NMR spectra were taken on an INOVA-400 spectrometer in DMSO-d_6 or $CDCl_3$ using tetramethylsilane (TMS) as an internal standard at room temperature. Elemental analysis was measured on a Vario EL III instrument. DSC measurements were conducted on a DSC 2010 under nitrogen at 10 °C min^{-1}. Mass spectra (MS) were measured with Ultraflextreme MALDI TOF/TOF spectroscope. The POM images of the target compounds were taken using a CPV-900C polarization microscope fitted with a Linkam LTS420 hot stage. The transition temperatures reported in this paper were the peak values of the transition on DSC traces. Few of them were the values obtained using POM. SAXS patterns were taken using an X-ray scattering instrument (SAXSess mc^2, Anton Paar) equipped with line collimation and a 2200 W sealed-tube X-ray generator (Cu-Kα, $\lambda = 0.154$ nm).

Chemicals

Dimethyl sulfoxide (DMSO) was obtained by distillation under reduced pressure. Tetrahydrofuran (THF) was distilled from sodium benzophenone ketyl in an atmosphere of nitrogen. Dicyclohexylcarbodiimde (DCC) was purchased from Shanghai

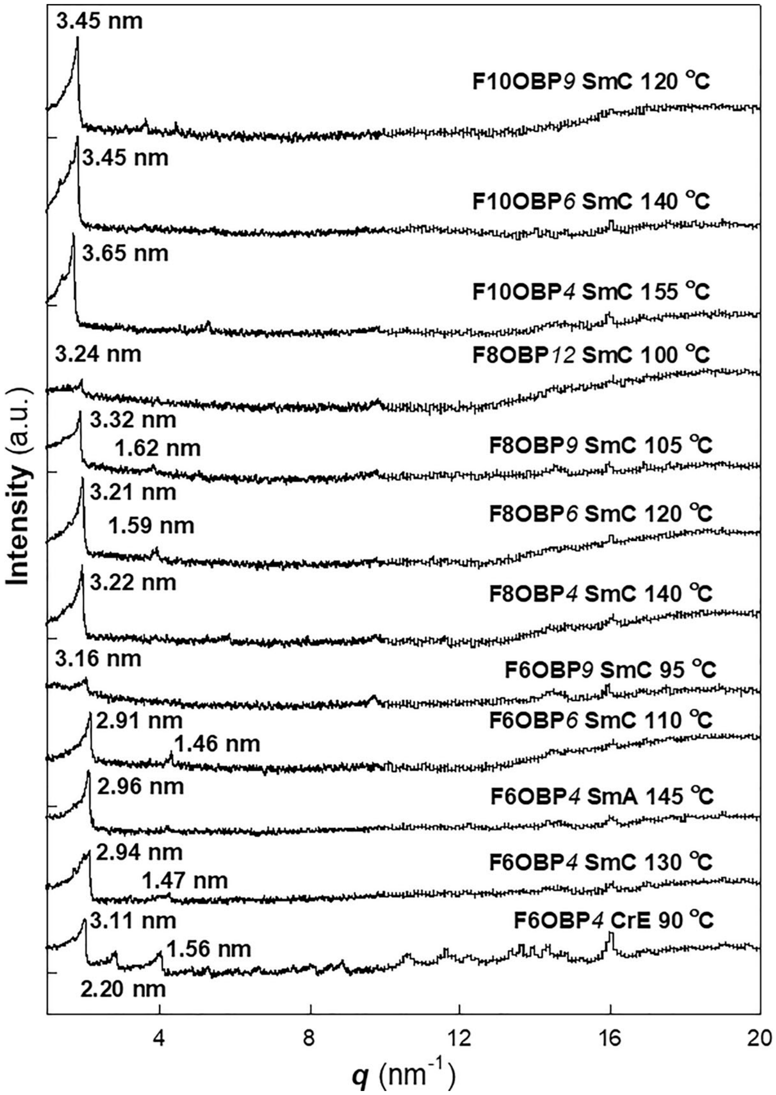

Figure 4. SAXS patterns of some liquid crystals taken at the different temperatures during the cooling process.

Aladdin Biotech Co., Ltd. (China). 4-Dimethylaminopyridine (DMAP) was purchased from Adamas Reagent Co., Ltd. (China). All other chemicals were purchased from Sinopharm Group Chemical Reagent Co., Ltd. (China) and used as received without further purification. 4-*n*-Alkoxybiphenyl-4′-carboxylic acids were synthesized according to the literature [23].

Synthesis

Synthesis of 3-perfluorohexylphenol

A typical synthetic procedure for the phenols was shown as following. To a suspension of 3-iodophenol (10 g, 45.5 mmol) and Cu powder (8.6 g, 136.4 mmol) in anhydrous

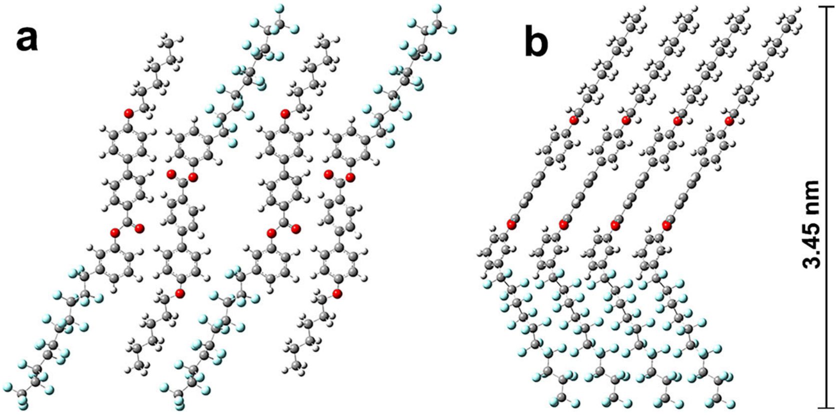

Figure 5. Simulated molecular packing structures of (a) **F10OBP***6* and (b) **F10OBP***9*.

DMSO (150.0 mL), perfluorohexyl iodide (24.3 g, 54.6 mmol) was added under N_2 and the mixture was stirred at 110 °C for 3 h. Precipitate was removed by filtration and washed with ether. After the addition of H_2O, the aqueous layer was extracted with ether. The combined layers were washed with H_2O and brine, and dried with anhydrous Na_2SO_4. After being filtered and concentrated, the residue was purified by column chromatography on silica gel (hexane/EtOAc, 10:1) to give product as a colorless oil; yield: 11.4 g (60.8%). FT-IR υ_{max}: 3397, 1199, 1142, and 849 cm^{-1}. ^1H NMR δ_H (400 MHz; DMSO-d_6; TMS): 6.99 (s, 1H, ArH), 7.08 (t, $J = 8.1$ Hz, 2H, ArH), 7.43 (t, $J = 7.9$ Hz, 1H, ArH), 10.13 (s, 1H, OH) ppm. MS m/z (rel. int.): 412 (M^+, 100).

Characterization of 3-perfluorooctylphenol

Yield: 12.3 g (52.8%). FT-IR υ_{max}: 3393, 1196, 1139 and 850 cm^{-1}. ^1H NMR δ_H (400 MHz; DMSO-d_6; TMS): 6.98 (s, 1H, ArH), 7.09 (t, $J = 8.1$ Hz, 2H, ArH), 7.43 (t, $J = 7.8$ Hz, 1H, ArH), 9.77 (s, 1H, OH) ppm. MS m/z (rel. int.): 512 (M^+, 100).

Characterization of 3-perfluorodecylphenol

Yield: 13.6 g (48.8%). FT-IR υ_{max}: 3400, 1197, 1145, and 846 cm^{-1}. ^1H NMR δ_H (400 MHz; DMSO-d_6; TMS): 6.97 (s, 1H, ArH), 7.09 (t, $J = 8.0$ Hz, 2H, ArH), 7.42 (t, $J = 7.9$ Hz, 1H, ArH), 9.37 (s, 1H, OH) ppm. MS m/z (rel. int.): 612 (M^+, 100).

Synthesis of F6OBP4

A typical synthetic procedure for the final compounds was shown as following. 4-*n*-Butoxybiphenyl-4′-carboxylic acid (67.5 mg, 0.25 mmol), 3-perfluorohexylphenol (103 mg, 0.25 mmol), DCC (57.7 mg, 0.28 mmol), catalytic DMAP and dry THF (20 ml) were stirred under N_2 at room temperature for 12 h. The mixture was filtered and the residue was washed with THF. The collected filtrates were evaporated on a rotary evaporator. The residue was recrystallized from acetone/methanol for two times to give 89 mg of white solid; yield 53.6%. FT-IR υ_{max}: 2933, 2872, 1739, 1602, 1500, 1191, 1139, and 826 cm^{-1}. ^1H NMR δ_H (400 MHz; $CDCl_3$; TMS): 0.95–1.87 (m, 7H, aliphatic hydrogens), 4.03 (t, $J = 6.4$ Hz, 2H, RCH_2O), 7.01 (d, $J = 8.3$ Hz, 2H, ArH), 7.52 (d,

$J = 10.1$ Hz, 3H, ArH), 7.60 (t, $J = 7.7$ Hz, 3H, ArH), 7.71 (d, $J = 8.0$ Hz, 2H, ArH), 8.24 (d, $J = 8.0$ Hz, 2H, ArH) ppm. MS *m/z* (rel. int.): 687(M^++Na, 100), 253($C_4H_9OC_6H_4C_6H_4CO^+$, 0.54). Elemental analysis: calculated (for $C_{29}H_{21}F_{13}O_3$), C 52.42, H 3.19%; found, C 52.71, H 3.49%.

Characterization of F6OBP5

Yield: 95.0 mg (56.0%). FT-IR υ_{max}: 2954, 2866, 1732, 1603, 1498, 1192, 1135, and 833 cm^{-1}. ^1H NMR δ_H (400 MHz; $CDCl_3$; TMS): 0.91–1.89 (m, 9H, aliphatic hydrogens), 4.03 (t, $J = 6.4$ Hz, 2H, RCH_2O), 7.01 (d, $J = 8.3$ Hz, 2H, ArH), 7.52 (d, $J = 10.1$ Hz, 3H, ArH), 7.60 (t, $J = 7.7$ Hz, 3H, ArH), 7.71 (d, $J = 8.0$ Hz, 2H, ArH), 8.24 (d, $J = 8.0$ Hz, 2H, ArH) ppm. MS *m/z* (rel. int.): 701(M^++Na, 100), 267($C_5H_{11}OC_6H_4C_6H_4CO^+$, 0.72). Elemental analysis: calculated (for $C_{30}H_{23}F_{13}O_3$), C 53.11, H 3.42%; found, C 53.37, H 3.56%.

Characterization of F6OBP6

Yield: 91.1 mg (52.7%). FT-IR υ_{max}: 2935, 2857, 1731, 1600, 1496, 1189, 1137, and 823 cm^{-1}. ^1H NMR δ_H (400 MHz; $CDCl_3$; TMS): 0.89–1.87 (m, 11H, aliphatic hydrogens), 4.03 (t, $J = 6.4$ Hz, 2H, RCH_2O), 7.01 (d, $J = 8.3$ Hz, 2H, ArH), 7.52 (d, $J = 10.1$ Hz, 3H, ArH), 7.60 (t, $J = 7.7$ Hz, 3H, ArH), 7.71 (d, $J = 8.0$ Hz, 2H, ArH), 8.24 (d, $J = 8.0$ Hz, 2H, ArH) ppm. MS *m/z* (rel. int.): 715(M^++Na, 100), 281($C_6H_{13}OC_6H_4C_6H_4CO^+$, 0.68). Elemental analysis: calculated (for $C_{31}H_{25}F_{13}O_3$), C 53.77, H 3.64%; found, C 54.00, H 3.83%.

Characterization of F6OBP7

Yield: 97.7 mg (55.4%). FT-IR υ_{max}: 2929, 2854, 1731, 1602, 1498, 1194, 1136, and 824 cm^{-1}. ^1H NMR δ_H (400 MHz; $CDCl_3$; TMS): 0.87–1.88 (m, 13H, aliphatic hydrogens), 4.03 (t, $J = 6.4$ Hz, 2H, RCH_2O), 7.01 (d, $J = 8.3$ Hz, 2H, ArH), 7.52 (d, $J = 10.1$ Hz, 3H, ArH), 7.60 (t, $J = 7.7$ Hz, 3H, ArH), 7.71 (d, $J = 8.0$ Hz, 2H, ArH), 8.24 (d, $J = 8.0$ Hz, 2H, ArH) ppm. MS *m/z* (rel. int.): 729(M^++Na, 100), 295($C_7H_{15}OC_6H_4C_6H_4CO^+$, 0.72). Elemental analysis: calculated (for $C_{32}H_{27}F_{13}O_3$), C 54.40, H 3.85%; found, C 54.46, H 3.96%.

Characterization of F6OBP8

Yield: 100.7 mg (55.9%). FT-IR υ_{max}: 2919, 2852, 1738, 1604, 1496, 1198, 1137 and 831 cm^{-1}. ^1H NMR δ_H (400 MHz; $CDCl_3$; TMS): 0.87-1.88 (m, 15H, aliphatic hydrogens), 4.03 (t, $J = 6.4$ Hz, 2H, RCH_2O), 7.01 (d, $J = 8.3$ Hz, 2H, ArH), 7.52 (d, $J = 10.1$ Hz, 3H, ArH), 7.60 (t, $J = 7.7$ Hz, 3H, ArH), 7.71 (d, $J = 8.0$ Hz, 2H, ArH), 8.24 (d, $J = 8.0$ Hz, 2H, ArH) ppm. MS m/z (rel. int.): 743(M^++Na, 100), 309($C_8H_{17}OC_6H_4C_6H_4CO^+$, 0.77). Elemental analysis: calculated (for $C_{33}H_{29}F_{13}O_3$), C 55.01, H 4.06%; found, C 55.31, H 3.35%.

Characterization of F6OBP9

Yield: 92.9 mg (50.6%). FT-IR υ_{max}: 2920, 2848, 1738, 1602, 1495, 1196, 1141, and 834 cm^{-1}. ^{1}H NMR δ_H (400 MHz; CDCl$_3$; TMS): 0.86–1.87 (m, 17H, aliphatic hydrogens), 4.03 (t, $J = 6.4$ Hz, 2H, RCH$_2$O), 7.01 (d, $J = 8.3$ Hz, 2H, ArH), 7.52 (d, $J = 10.1$ Hz, 3H, ArH), 7.60 (t, $J = 7.7$ Hz, 3H, ArH), 7.71 (d, $J = 8.0$ Hz, 2H, ArH), 8.24 (d, $J = 8.0$ Hz, 2H, ArH) ppm. MS *m/z* (rel. int.): 757(M^++Na, 100), 323($C_9H_{19}OC_6H_4C_6H_4CO^+$, 0.70). Elemental analysis: calculated (for $C_{34}H_{31}F_{13}O_3$), C 55.59, H 4.25%; found, C 55.89, H 4.43%.

Characterization of F6OBP10

Yield: 97.2 mg (52.0%). FT-IR υ_{max}: 2917, 2850, 1737, 1603, 1495, 1194, 1146, and 833 cm^{-1}. ^{1}H NMR δ_H (400 MHz; CDCl$_3$; TMS): 0.86–1.87 (m, 19H, aliphatic hydrogens), 4.03 (t, $J = 6.4$ Hz, 2H, RCH$_2$O), 7.01 (d, $J = 8.3$ Hz, 2H, ArH), 7.52 (d, $J = 10.1$ Hz, 3H, ArH), 7.60 (t, $J = 7.7$ Hz, 3H, ArH), 7.71 (d, $J = 8.0$ Hz, 2H, ArH), 8.24 (d, $J = 8.0$ Hz, 2H, ArH) ppm. MS *m/z* (rel. int.): 771(M^++Na, 100), 337($C_{10}H_{21}OC_6H_4C_6H_4CO^+$, 0.61). Elemental analysis: calculated (for $C_{35}H_{33}F_{13}O_3$), C 56.15, H 4.44%; found, C 56.43, H 4.70%.

Characterization of F6OBP12

Yield: 99.8 mg (51.4%). FT-IR υ_{max}: 2918, 2848, 1738, 1604, 1495, 1196, 1142, and 829 cm^{-1}. ^{1}H NMR δ_H (400 MHz; CDCl$_3$; TMS): 0.85–1.87 (m, 23H, aliphatic hydrogens), 4.03 (t, $J = 6.4$ Hz, 2H, RCH$_2$O), 7.01 (d, $J = 8.3$ Hz, 2H, ArH), 7.52 (d, $J = 10.1$ Hz, 3H, ArH), 7.60 (t, $J = 7.7$ Hz, 3H, ArH), 7.71 (d, $J = 8.0$ Hz, 2H, ArH), 8.24 (d, $J = 8.0$ Hz, 2H, ArH) ppm. MS *m/z* (rel. int.): 799(M^++Na, 100), 365($C_{12}H_{25}OC_6H_4C_6H_4CO^+$, 0.68). Elemental analysis: calculated (for $C_{37}H_{37}F_{13}O_3$), C 57.22, H 4.80%; found, C 57.33, H 4.90%.

Characterization of F8OBP4

Yield: 108.5 mg (56.8%). FT-IR υ_{max}: 2937, 2868, 1731, 1604, 1495, 1194, 1144 and 827 cm^{-1}. ^{1}H NMR δ_H (400 MHz; CDCl$_3$; TMS): 0.96-1.87 (m, 7H, aliphatic hydrogens), 4.03 (t, $J = 5.8$ Hz, 2H, RCH$_2$O), 7.01 (d, $J = 8.0$ Hz, 2H, ArH), 7.50 (s, 1H, ArH), 7.52 (d, $J = 9.9$ Hz, 2H, ArH), 7.60 (t, $J = 6.0$ Hz, 1H, ArH), 7.61 (d, $J = 7.8$ Hz, 2H, ArH), 7.71 (d, $J = 7.7$ Hz, 2H, ArH), 8.24 (d, $J = 7.7$ Hz, 2H, ArH) ppm. MS m/z (rel. int.): 787(M^++Na, 100), 253($C_4H_9OC_6H_4C_6H_4CO^+$, 0.72). Elemental analysis: calculated (for $C_{31}H_{21}F_{17}O_3$), C 48.70, H 2.77%; found, C 48.72, H 3.08%.

Characterization of F8OBP5

Yield: 106.8 mg (54.9%). FT-IR υ_{max}: 2938, 2858, 1730, 1602, 1495, 1195, 1143 and 825 cm^{-1}. ^{1}H NMR δ_H (400 MHz; CDCl$_3$; TMS): 0.91-1.89 (m, 9H, aliphatic hydrogens), 4.02 (t, $J = 5.9$ Hz, 2H, RCH$_2$O), 7.01 (d, $J = 8.0$ Hz, 2H, ArH), 7.50 (s, 1H, ArH), 7.52 (d, $J = 9.7$ Hz, 2H, ArH), 7.60 (t, $J = 6.0$ Hz, 1H, ArH), 7.61 (d, $J = 7.8$ Hz, 2H, ArH), 7.71 (d, $J = 7.6$ Hz, 2H, ArH), 8.24 (d, $J = 7.7$ Hz, 2H, ArH) ppm. MS m/z (rel. int.): 801(M^++Na, 100), 267($C_5H_{11}OC_6H_4C_6H_4CO^+$, 0.76). Elemental analysis: calculated (for $C_{32}H_{23}F_{17}O_3$), C 49.37, H 2.98%; found, C 49.82, H 3.42%.

Characterization of F8OBP6

Yield: 105.7 mg (53.4%). FT-IR υ_{max}: 2936, 2858, 1731, 1603, 1497, 1197, 1146, and 827 cm^{-1}. ^{1}H NMR δ_H (400 MHz; CDCl$_3$; TMS): 0.89–1.87 (m, 11H, aliphatic hydrogens), 4.02 (t, $J = 6.5$ Hz, 2H, RCH$_2$O), 7.01 (d, $J = 8.6$ Hz, 2H, ArH), 7.50 (s, 1H, ArH), 7.52 (d, $J = 10.4$ Hz, 2H, ArH), 7.60 (t, $J = 6.0$ Hz, 1H, ArH), 7.61 (d, $J = 7.7$ Hz, 2H, ArH), 7.71 (d, $J = 8.2$ Hz, 2H, ArH), 8.24 (d, $J = 8.2$ Hz, 2H, ArH) ppm. MS *m/z* (rel. int.): 815(M$^+$+Na, 100), 281($C_6H_{13}OC_6H_4C_6H_4CO^+$, 0.84). Elemental analysis: calculated (for $C_{33}H_{25}F_{17}O_3$), C 50.01, H 3.18%; found, C 50.51, H 3.54%.

Characterization of F8OBP7

Yield: 109.9 mg (54.5%). FT-IR υ_{max}: 2916, 2851, 1737, 1603, 1496, 1195, 1145, and 834 cm^{-1}. ^{1}H NMR δ_H (400 MHz; CDCl$_3$; TMS): 0.86–1.87 (m, 13H, aliphatic hydrogens), 4.01 (t, $J = 6.1$ Hz, 2H, RCH$_2$O), 7.01 (d, $J = 8.2$ Hz, 2H, ArH), 7.50 (s, 1H, ArH), 7.52 (d, $J = 10.6$ Hz, 2H, ArH), 7.60 (t, $J = 6.0$ Hz, 1H, ArH), 7.61 (d, $J = 8.0$ Hz, 2H, ArH), 7.71 (d, $J = 8.0$ Hz, 2H, ArH), 8.24 (d, $J = 7.9$ Hz, 2H, ArH) ppm. MS *m/z* (rel. int.): 829(M$^+$+Na, 100), 295($C_7H_{15}OC_6H_4C_6H_4CO^+$, 0.72). Elemental analysis: calculated (for $C_{33}H_{25}F_{17}O_3$), C 50.63, H 3.37%; found, C 50.41, H 3.59%.

Characterization of F8OBP8

Yield: 115.4 mg (56.3%). FT-IR υ_{max}: 2916, 2849, 1739, 1601, 1497, 1192, 1146, and 829 cm^{-1}. ^{1}H NMR δ_H (400 MHz; CDCl$_3$; TMS): 0.86–1.87 (m, 15H, aliphatic hydrogens), 4.02 (t, $J = 6.0$ Hz, 2H, RCH$_2$O), 7.01 (d, $J = 8.2$ Hz, 2H, ArH), 7.50 (s, 1H, ArH), 7.52 (d, $J = 10.4$ Hz, 2H, ArH), 7.60 (t, $J = 6.0$ Hz, 1H, ArH), 7.61 (d, $J = 7.8$ Hz, 2H, ArH), 7.71 (d, $J = 7.8$ Hz, 2H, ArH), 8.24 (d, $J = 7.7$ Hz, 2H, ArH) ppm. MS *m/z* (rel. int.): 843(M$^+$+Na, 100), 309($C_8H_{17}OC_6H_4C_6H_4CO^+$, 0.76). Elemental analysis: calculated (for $C_{33}H_{25}F_{17}O_3$), C 51.23, H 3.56%; found, C 51.62, H 3.85%.

Characterization of F8OBP9

Yield: 111.0 mg (53.2%). FT-IR υ_{max}: 2918, 2851, 1738, 1601, 1497, 1193, 1144, and 833 cm^{-1}. ^{1}H NMR δ_H (400 MHz; CDCl$_3$; TMS): 0.86–1.87 (m, 17H, aliphatic hydrogens), 4.02 (t, $J = 6.5$ Hz, 2H, RCH$_2$O), 7.01 (d, $J = 8.4$ Hz, 2H, ArH), 7.50 (s, 1H, ArH), 7.52 (d, $J = 10.7$ Hz, 2H, ArH), 7.60 (t, $J = 6.0$ Hz, 1H, ArH), 7.61 (d, $J = 7.6$ Hz, 2H, ArH), 7.71 (d, $J = 8.1$ Hz, 2H, ArH), 8.24 (d, $J = 8.1$ Hz, 2H, ArH) ppm. MS *m/z* (rel. int.): 857(M$^+$+Na, 100), 323($C_9H_{19}OC_6H_4C_6H_4CO^+$, 0.64). Elemental analysis: calculated (for $C_{33}H_{25}F_{17}O_3$), C 51.81, H 3.74%; found, C 51.62, H 4.02%.

Characterization of F8OBP10

Yield: 114.6 mg (54.1%). FT-IR υ_{max}: 2916, 2849, 1740, 1602, 1496, 1193, 1146, and 835 cm^{-1}. ^{1}H NMR δ_H (400 MHz; CDCl$_3$; TMS): 0.86–1.87 (m, 19H, aliphatic hydrogens), 4.02 (t, $J = 6.1$ Hz, 2H, RCH$_2$O), 7.01 (d, $J = 8.1$ Hz, 2H, ArH), 7.50 (s, 1H, ArH), 7.52 (d, $J = 10.5$ Hz, 2H, ArH), 7.60 (t, $J = 6.0$ Hz, 1H, ArH), 7.61 (d, $J = 7.7$ Hz, 2H, ArH), 7.71 (d, $J = 7.8$ Hz, 2H, ArH), 8.24 (d, $J = 7.7$ Hz, 2H, ArH) ppm. MS *m/z* (rel.

int.): 871(M^++Na, 100), 337($C_{10}H_{21}OC_6H_4C_6H_4CO^+$, 0.73). Elemental analysis: calculated (for $C_{33}H_{25}F_{17}O_3$), C 52.37, H 3.92%; found, C 52.69, H 4.15%.

Characterization of F8OBP12

Yield: 115.5 mg (52.7%). FT-IR υ_{max}: 2918, 2852, 1739, 1602, 1495, 1193, 1147, and 828 cm^{-1}. ^1H NMR δ_H (400 MHz; $CDCl_3$; TMS): 0.85–1.87 (m, 23H, aliphatic hydrogens), 4.02 (t, $J=6.4$ Hz, 2H, RCH_2O), 7.01 (d, $J=8.5$ Hz, 2H, ArH), 7.50 (s, 1H, ArH), 7.52 (d, $J=10.4$ Hz, 2H, ArH), 7.60 (t, $J=6.0$ Hz, 1H, ArH), 7.61 (d, $J=7.5$ Hz, 2H, ArH), 7.71 (d, $J=8.2$ Hz, 2H, ArH), 8.24 (d, $J=8.2$ Hz, 2H, ArH) ppm. MS *m/z* (rel. int.): 899(M^++Na, 100), 365($C_{12}H_{25}OC_6H_4C_6H_4CO^+$, 0.62). Elemental analysis: calculated (for $C_{33}H_{25}F_{17}O_3$), C 53.43, H 4.25%; found, C 53.86, H 4.53%.

Characterization of F10OBP4

Yield: 118.4 mg (54.8%). FT-IR υ_{max}: 2936, 2868, 1731, 1604, 1497, 1195, 1148, and 825 cm^{-1}. ^1H NMR δ_H (400 MHz; $CDCl_3$; TMS): 0.97–1.86 (m, 7H, aliphatic hydrogens), 4.03 (t, $J=6.4$ Hz, 2H, RCH_2O), 7.01 (d, $J=8.6$ Hz, 2H, ArH), 7.50 (s, 1H, ArH), 7.52 (d, $J=10.7$ Hz, 2H, ArH), 7.60 (t, $J=6.0$ Hz, 1H, ArH), 7.61 (d, $J=7.8$ Hz, 2H, ArH), 7.71 (d, $J=8.2$ Hz, 2H, ArH), 8.24 (d, $J=8.2$ Hz, 2H, ArH) ppm. MS *m/z* (rel. int.): 887(M^++Na, 100), 253($C_4H_9OC_6H_4C_6H_4CO^+$, 0.84). Elemental analysis: calculated (for $C_{33}H_{21}F_{21}O_3$), C 45.85, H 2.45%; found, C 45.80, H 2.66%.

Characterization of F10OBP5

Yield: 114.9 mg (52.3%). FT-IR υ_{max}: 2939, 2874, 1731, 1601, 1497, 1194, 1148, and 826 cm^{-1}. ^1H NMR δ_H (400 MHz; $CDCl_3$; TMS): 0.92–1.88 (m, 9H, aliphatic hydrogens), 4.02 (t, $J=6.5$ Hz, 2H, RCH_2O), 7.01 (d, $J=8.7$ Hz, 2H, ArH), 7.50 (s, 1H, ArH), 7.52 (d, $J=10.4$ Hz, 2H, ArH), 7.60 (t, $J=6.0$ Hz, 1H, ArH), 7.61 (d, $J=7.6$ Hz, 2H, ArH), 7.71 (d, $J=8.2$ Hz, 2H, ArH), 8.24 (d, $J=8.2$ Hz, 2H, ArH) ppm. MS *m/z* (rel. int.): 901(M^++Na, 100), 267($C_5H_{11}OC_6H_4C_6H_4CO^+$, 0.76). Elemental analysis: calculated (for $C_{34}H_{23}F_{21}O_3$), C 46.48, H 2.64%; found, C 46.41, H 3.00%.

Characterization of F10OBP6

Yield: 119.8 mg (53.7%). FT-IR υ_{max}: 2938, 2859, 1729, 1601, 1495, 1194, 1145, and 826 cm^{-1}. ^1H NMR δ_H (400 MHz; $CDCl_3$; TMS): 0.89–1.87 (m, 11H, aliphatic hydrogens), 4.02 (t, $J=6.5$ Hz, 2H, RCH_2O), 7.01 (d, $J=8.6$ Hz, 2H, ArH), 7.50 (s, 1H, ArH), 7.52 (d, $J=10.6$ Hz, 2H, ArH), 7.60 (t, $J=6.0$ Hz, 1H, ArH), 7.61 (d, $J=7.7$ Hz, 2H, ArH), 7.71 (d, $J=8.2$ Hz, 2H, ArH), 8.24 (d, $J=8.2$ Hz, 2H, ArH) ppm. MS *m/z* (rel. int.): 915(M^++Na, 100), 281($C_6H_{13}OC_6H_4C_6H_4CO^+$, 0.63). Elemental analysis: calculated (for $C_{35}H_{25}F_{21}O_3$), C 47.10, H 2.82%; found, C 47.28, H 3.19%.

Characterization of F10OBP7

Yield: 119.5 mg (52.8%). FT-IR υ_{max}: 2921, 2855, 1732, 1604, 1498, 1193, 1149, and 826 cm^{-1}. ^1H NMR δ_H (400 MHz; $CDCl_3$; TMS): 0.87–1.87 (m, 13H, aliphatic hydrogens), 4.02 (t, $J=6.5$ Hz, 2H, RCH_2O), 7.01 (d, $J=8.8$ Hz, 2H, ArH), 7.50 (s, 1H, ArH), 7.52 (d, $J = 10.5$ Hz, 2H, ArH), 7.60 (t, $J = 6.0$ Hz, 1H, ArH), 7.61 (d, $J = 8.4$ Hz, 2H, ArH), 7.71 (d, $J = 8.2$ Hz, 2H, ArH), 8.24 (d, $J = 8.2$ Hz, 2H, ArH) ppm. MS *m/z* (rel. int.): 929(M^++Na, 100), 295($C_7H_{15}OC_6H_4C_6H_4CO^+$, 0.72). Elemental analysis: calculated (for $C_{31}H_{21}F_{17}O_3$), C 47.69, H 3.00%; found, C 47.70, H 3.42%.

Characterization of F10OBP8

Yield: 124.9 mg (54.3%). FT-IR υ_{max}: 2922, 2855, 1724, 1602, 1497, 1195, 1148, and 829 cm^{-1}. ^1H NMR δ_H (400 MHz; $CDCl_3$; TMS): 0.87–1.87 (m, 15H, aliphatic hydrogens), 4.02 (t, $J = 6.5$ Hz, 2H, RCH_2O), 7.01 (d, $J = 8.5$ Hz, 2H, ArH), 7.50 (s, 1H, ArH), 7.52 (d, $J = 10.5$ Hz, 2H, ArH), 7.60 (t, $J = 6.0$ Hz, 1H, ArH), 7.61 (d, $J = 8.3$ Hz, 2H, ArH), 7.71 (d, $J = 7.9$ Hz, 2H, ArH), 8.24 (d, $J = 8.2$ Hz, 2H, ArH) ppm. MS *m/z* (rel. int.): 943(M^++Na, 100), 309($C_8H_{17}OC_6H_4C_6H_4CO^+$, 0.62). Elemental analysis: calculated (for $C_{31}H_{21}F_{17}O_3$), C 48.27, H 3.18%; found, C 48.32, H 3.51%.

Characterization of F10OBP9

Yield: 120.6 mg (51.6%). FT-IR υ_{max}: 2921, 2854, 1739, 1602, 1497, 1193, 1148, and 828 cm^{-1}. ^1H NMR δ_H (400 MHz; $CDCl_3$; TMS): 0.85–1.87 (m, 17H, aliphatic hydrogens), 4.02 (t, $J = 6.5$ Hz, 2H, RCH_2O), 7.01 (d, $J = 8.5$ Hz, 2H, ArH), 7.50 (s, 1H, ArH), 7.52 (d, $J = 10.5$ Hz, 2H, ArH), 7.60 (t, $J = 6.0$ Hz, 1H, ArH), 7.61 (d, $J = 7.7$ Hz, 2H, ArH), 7.71 (d, $J = 8.2$ Hz, 2H, ArH), 8.24 (d, $J = 8.2$ Hz, 2H, ArH) ppm. MS *m/z* (rel. int.): 957(M^++Na, 100), 323($C_9H_{19}OC_6H_4C_6H_4CO^+$, 0.76). Elemental analysis: calculated (for $C_{31}H_{21}F_{17}O_3$), C 48.83, H 3.34%; found, C 49.16, H 3.72%.

Characterization of F10OBP10

Yield: 120.1 mg (50.7%). FT-IR υ_{max}: 2923, 2851, 1734, 1605, 1497, 1191, 1148, and 828 cm^{-1}. ^1H NMR δ_H (400 MHz; $CDCl_3$; TMS): 0.84–1.87 (m, 19H, aliphatic hydrogens), 4.02 (t, $J = 6.4$ Hz, 2H, RCH_2O), 7.01 (d, $J = 8.5$ Hz, 2H, ArH), 7.50 (s, 1H, ArH), 7.52 (d, $J = 10.3$ Hz, 2H, ArH), 7.60 (t, $J = 6.0$ Hz, 1H, ArH), 7.61 (d, $J = 7.7$ Hz, 2H, ArH), 7.71 (d, $J = 8.2$ Hz, 2H, ArH), 8.24 (d, $J = 8.1$ Hz, 2H, ArH) ppm. MS *m/z* (rel. int.): 971(M^++Na, 100), 337($C_{10}H_{21}OC_6H_4C_6H_4CO^+$, 0.74). Elemental analysis: calculated (for $C_{31}H_{21}F_{17}O_3$), C 49.38, H 3.51%; found, C 49.73, H 3.89%.

Characterization of F10OBP12

Yield: 123.7 mg (50.7%). FT-IR υ_{max}: 2916, 2849, 1738, 1604, 1495, 1194, 1149, and 828 cm^{-1}. ^1H NMR δ_H (400 MHz; $CDCl_3$; TMS): 0.85–1.87 (m, 23H, aliphatic hydrogens), 4.02 (t, $J = 6.5$ Hz, 2H, RCH_2O), 7.01 (d, $J = 8.5$ Hz, 2H, ArH), 7.50 (s, 1H, ArH), 7.52 (d, $J = 10.5$ Hz, 2H, ArH), 7.60 (t, $J = 6.0$ Hz, 1H, ArH), 7.61 (d, $J = 7.7$ Hz, 2H, ArH), 7.71 (d, $J = 8.2$ Hz, 2H, ArH), 8.24 (d, $J = 8.2$ Hz, 2H, ArH) ppm. MS *m/z* (rel. int.): 999(M^++Na, 100), 365($C_{12}H_{25}OC_6H_4C_6H_4CO^+$, 0.68). Elemental analysis: calculated (for $C_{31}H_{21}F_{17}O_3$), C 50.42, H 3.82%; found, C 50.76, H 4.07%.

Funding

This work was supported the Political Science-Preponderant Discipline of Jiangsu Province, the Project of Scientific and Technologic Infrastructure of Suzhou (SZS201905) and the National Natural Science Foundation of China (No. 51473141 and 21574095).

ORCID

Yonggang Yang http://orcid.org/0000-0003-0185-7471

References

[1] H. T. Nguyen *et al.*, *Liq. Cryst.* **10** (3), 389 (1991). doi:10.1080/02678299108026285

[2] P. Kromm *et al.*, *Liq. Cryst.* **21** (1), 121 (1996). doi:10.1080/02678299608033802

[3] F. G. Tournilhac *et al.*, *Nature* **359** (6396), 621 (1992). doi:10.1038/359621a0

[4] H. Liu, and H. Nohira, *Liq. Cryst.* **22** (2), 217 (1997). doi:10.1080/026782997209595

[5] S. V. Arehart, and C. Pugh, *J. Am. Chem. Soc.* **119** (13), 3027 (1997). doi:10.1021/ja963687p

[6] H. Hird, *Chem. Soc. Rev.* **36** (12), 2070 (2007). doi:10.1039/b610738a

[7] H. Li, J. Wen, and Y. Yang, *Mol. Cryst. Liq. Cryst.* **473** (1), 15 (2007). doi:10.1080/15421400701613458

[8] Y. Yang, H. Li, and J. Wen, *Liq. Cryst.* **34** (10), 1167 (2007). doi:10.1080/02678290701663829

[9] P. Kirsch, *J. Fluor. Chem.* **177**, 29 (2015). doi:10.1016/j.jfluchem.2015.01.007

[10] M. Kohout *et al.*, *Liq. Cryst.* **43** (10), 1472 (2016). doi:10.1080/02678292.2016.1185170

[11] V. Novotná *et al.*, *Liq. Cryst.* **43** (9), 1251 (2016). doi:10.1080/02678292.2016.1166402

[12] S. Marzouk *et al.*, *J. Fluor. Chem.* **197**, 15 (2017). doi:10.1016/j.jfluchem.2017.02.006

[13] V. Kumar *et al.*, *J. Fluor. Chem.* **198**, 54 (2017). doi:10.1016/j.jfluchem.2016.12.011

[14] J. Du, X. Wang, and G. Zou, *J. Therm. Anal. Calorim.* **129** (1), 467 (2017). doi:10.1007/s10973-017-6171-1

[15] X. Cheng *et al.*, *J. Am. Chem. Soc.* **126** (40), 12930 (2004). doi:10.1021/ja048224v

[16] X. Cheng *et al.*, *J. Am. Chem. Soc.* **133** (20), 7872 (2011). doi:10.1021/ja200822z

[17] C. Tschierske, *Angew. Chem. Int. Ed. Engl.* **52** (34), 8828 (2013). doi:10.1002/anie.201300872

[18] M. Prehm *et al.*, *Angew. Chem. Int. Ed. Engl.* **46** (42), 7972 (2007). doi:10.1002/anie.200703171

[19] G. Jin *et al.*, *Liq. Cryst.* **45**, 594 (2018).

[20] Y.-G. Yang, K. Wang, and J. X. Wen, *Liq. Cryst.* **28** (10), 1553 (2001). doi:10.1080/02678290110071538

[21] P. Kromm, M. Cotrait, and H. T. Nguyen, *Liq. Cryst.* **21** (1), 95 (1996). doi:10.1080/02678299608033799

[22] T. Doi *et al.*, *J. Mater. Chem.* **1** (2), 169 (1991). doi:10.1039/jm9910100169

[23] S.-L. Wu, and C.-Y. Lin, *Liq. Cryst.* **30** (4), 471 (2003). doi:10.1080/0267829031000089898